energies

MDPI

Article

A Physics-Informed Deep Learning Method for Wind Turbine Impedance Modeling

Libin Wen [1,2], Jinji Xi [1,2], Tannan Xiao [3,*], Hong Hu [1,2] and Ying Chen [4]

[1] Electric Power Research Institute of Guangxi Power Grid Co., Ltd., Nanning 530032, China
[2] Guangxi Key Laboratory of Intelligent Control and Maintenance of Power Equipment, Nanning 530032, China
[3] State Key Laboratory of Power System Operation and Control, Tsinghua University, Beijing 100084, China
[4] Department of Electrical Engineering, Tsinghua University, Beijing 100084, China
* Correspondence: xiaotn@mail.tsinghua.edu.cn

Abstract

Accurate impedance modeling of wind turbines (WTs) is essential for assessing the small-signal stability of power systems with high penetration of renewable energy. Existing approaches face a fundamental trade-off: physics-based "white-box" models require proprietary manufacturer parameters that are rarely disclosed, while purely data-driven "black-box" models often lack physical interpretability and exhibit poor generalization under unseen operating conditions. To address this gap, this paper proposes a gray-box framework—the Physics-Informed Hybrid Model (PIHM)—that integrates a simplified physical impedance branch with a Bidirectional Long Short-Term Memory (Bi-LSTM) network in a novel parallel architecture. The physical branch, systematically parameterized via a constrained phase-error minimization method, captures the dominant baseline dynamics and decouples the learning task, allowing the Bi-LSTM to focus exclusively on the complex nonlinear residual. The framework is validated on a high-fidelity simulation platform of a doubly fed induction generator (DFIG) wind farm. Quantitative results demonstrate that the PIHM achieves an average coefficient of determination (R^2) of 0.989 and a mean squared error (MSE) of 1.24×10^{-4} on unseen test data, while producing smooth, physically consistent impedance profiles that generalize across four distinct wind speed conditions. These results establish the PIHM as a reliable, parameter-free tool for impedance-based stability analysis of modern wind power systems.

Keywords: wind farm; wind turbine; impedance modeling; physics-informed neural network; LSTM; gray-box model

Check for updates

Academic Editor: Fue-Sang Lien

Received: 14 May 2026
Revised: 21 June 2026
Accepted: 26 June 2026
Published: 30 June 2026

Copyright: © 2026 by the authors. Licensee MDPI, Basel, Switzerland. This article is an open access article distributed under the terms and conditions of the Creative Commons Attribution (CC BY) license.

1. Introduction

The global energy landscape is undergoing a profound transformation, with wind power emerging as a central pillar in the pursuit of a sustainable, low-carbon future. The Global Wind Energy Council reports a continuous and rapid increase in installed capacity, highlighting the critical role of wind energy in meeting international climate targets [1,2]. Recent advances further underscore this trend, encompassing large-scale offshore wind resource assessments [3] and the integration of wind generation into complex multi-energy systems [4], both of which heighten the demand for accurate and reliable wind turbine models. This large-scale integration, however, introduces unprecedented challenges to the stability and security of electrical grids [5]. Unlike conventional synchronous generators with inherent inertial response, modern wind turbines (WTs) interface with the grid

through power electronic converters. The complex and fast-acting control dynamics of these converters fundamentally alter the system's dynamic behavior [6]. This alteration gives rise to new forms of instability, particularly subsynchronous oscillations (SSOs), which have been extensively reviewed and identified as a major operational risk [7,8]. Such oscillations, occurring at frequencies below the grid's nominal frequency, can lead to severe equipment damage and widespread blackouts, making their analysis and mitigation a critical research imperative [9,10].

Impedance-based stability analysis, grounded in the Nyquist stability criterion, has become the state-of-the-art method for investigating these converter-driven stability issues [11]. This frequency-domain technique models the system as two interconnected subsystems at the point of common coupling (PCC): the wind turbine and the grid. System stability can then be assessed by analyzing the impedance ratio of these two subsystems [12]. The success of this method is fundamentally contingent upon the availability of an accurate, wide-band impedance model of the wind turbine. This critical dependency has spurred extensive research into WT impedance modeling, which can be broadly categorized into three main paradigms: white-box, black-box, and gray-box models.

The "white-box," or physics-based, approach involves developing a detailed analytical model from first principles. This requires a comprehensive understanding of the turbine's aerodynamics, mechanical drivetrain, and electrical subsystems, as well as the intricate details of its multi-loop control system. Seminal works have derived detailed state-space and transfer function models for doubly fed induction generators (DFIGs) [13] and Permanent-Magnet Synchronous Generators (PMSGs) [14,15]. While these models offer high interpretability and provide deep insight into the physical mechanisms of oscillation, they share a critical, often insurmountable, drawback in practice. Their accuracy is highly dependent on precise knowledge of the turbine's internal design specifications and control parameters, such as controller gains, time constants, and protection logic thresholds [16]. These parameters are considered proprietary intellectual property by manufacturers and are rarely disclosed, which severely limits the applicability of white-box models for real-world systems [17,18].

To overcome the parameter-dependency of white-box models, "black-box" data-driven techniques have gained significant prominence [19]. These methods treat the wind turbine as an unknown system and identify its terminal characteristics solely from measurement data. Early approaches utilized system identification techniques such as sweep frequency response analysis (SFRA) to build an empirical model from perturbation tests [20]. More recently, machine learning has shown immense promise. Foundational work in machine learning for wireless networks and general applications has demonstrated the power of Artificial Neural Networks (ANNs) in approximating complex, nonlinear functions [21,22]. In the power systems domain, this has been adapted to model WT dynamics. Given the time-series nature of the voltage and current signals, Recurrent Neural Networks (RNNs) and their advanced variant, Long Short-Term Memory (LSTM) networks, have proven especially effective [23]. LSTM networks are explicitly designed to learn long-term temporal dependencies, making them ideal for forecasting wind power [24] and modeling the dynamic response of WTs [25]. Despite their success in fitting training data, purely black-box models are not a panacea. They often lack physical interpretability and can struggle with generalization, as their performance degrades when faced with operating conditions not well represented in the training dataset. This has been noted in broader data-driven applications like wind turbine condition monitoring [26,27].

This has led to the emergence of a third paradigm, "gray-box" or physics-informed modeling, which seeks to synergize the strengths of both approaches. This field leverages prior physical knowledge to constrain or guide the machine learning process, improving

data efficiency and promoting physically plausible solutions [28]. For impedance modeling specifically, hybrid approaches that combine simplified physical circuits with neural networks are beginning to be explored. For instance, Rao et al. proposed a combined knowledge-driven and data-driven method for online impedance identification [29]. Similarly, Wang et al. developed a data-driven impedance model for DFIGs, showing the potential of these methods [30]. However, the optimal architecture for such a hybrid model, particularly a systematic method for parameterizing the physical component and structuring the learning process for maximum efficiency, remains an open and compelling research question.

To bridge this gap, this paper proposes a novel gray-box framework for wind turbine impedance modeling, featuring a physics-informed Bidirectional LSTM (Bi-LSTM) network. The approach is designed to be accurate, robust, and interpretable, without requiring access to proprietary manufacturer data. Existing hybrid approaches, such as those in [29,30], demonstrate the feasibility of combining physical knowledge with data-driven methods but leave open key questions regarding the optimal parallel architecture design, the systematic parameterization of the physical component, and the structured decomposition of the learning task. This paper addresses these open questions. The main contributions of this work are three-fold:

- A Novel Parallel Hybrid Architecture: A unique parallel structure is proposed where a physical impedance branch and a Bi-LSTM network operate concurrently. Unlike series or simple constraint-based models, this architecture guarantees a physically grounded baseline response while enabling a structured decoupled learning strategy.
- A Decoupled Residual Learning Strategy: The physical branch is designed to model the dominant, low-frequency dynamics of the turbine. This decouples the learning task, allowing the Bi-LSTM to focus its capacity solely on modeling the complex, nonlinear residual dynamics. This division of labor promotes faster convergence, better final accuracy, and a more robust overall model.
- A Systematic Method for Physical Parameter Identification: A data-driven, grid-search-based method is introduced to parameterize the physical branch without requiring manufacturer data. By minimizing the phase error under a magnitude constraint, this method provides a robust and reproducible foundation for the hybrid model, supporting its generalization capabilities.

The remainder of this paper is organized as follows. Section 2 presents the theoretical background and formally defines the problem. Section 3 details the proposed physics-informed hybrid modeling framework. Section 4 presents a comprehensive case study. Section 5 concludes the paper and discusses potential avenues for future research.

2. Theoretical Background and Problem Formulation

This section first reviews the fundamental principles of impedance measurement and the architecture of Long Short-Term Memory (LSTM) networks, which are the building blocks of the proposed method. Subsequently, a formal mathematical definition of the wind turbine impedance modeling problem is provided.

2.1. Impedance-Based Stability and Measurement

Impedance-based stability analysis is a frequency-domain method that treats a power system as two interacting subsystems at the point of common coupling (PCC): a source subsystem (e.g., the wind turbine) and a load subsystem (e.g., the main grid). The system is stable if the ratio of the two impedances satisfies the Nyquist stability criterion [31]. Therefore, obtaining the turbine's impedance, $Z_{wt}(\omega)$, is paramount.

In a setting where internal parameters are unknown, the turbine's impedance must be identified from terminal measurements. This is typically achieved by injecting a small-

signal voltage or current perturbation at various frequencies and measuring the system's response. The impedance at a specific frequency, f, is defined as the ratio of the phasor of the terminal voltage, $\dot{V}(f)$, to the phasor of the terminal current, $\dot{I}(f)$. When considering a voltage source $\dot{V}_{in}(f)$ connected to the PCC through a line impedance, the resulting impedance of the wind turbine, $\dot{Z}_{wt}(f)$, can be calculated from the measured voltage at the PCC, $\dot{V}_{pcc}(f)$, as follows:

$$\dot{Z}_{wt}(f) = \frac{\dot{V}_{pcc}(f)}{\dot{I}_{pcc}(f)} = \frac{\dot{V}_{pcc}(f)}{(\dot{V}_{in}(f) - \dot{V}_{pcc}(f))/Z_{line}(f)} \quad (1)$$

The data-driven context, which aims to model the turbine as an unknown system, is simplified to the direct relationship between the PCC voltage and the resulting current response from the turbine. The fundamental task is to accurately predict the current phasor $\dot{I}_{pcc}(f)$ given the voltage phasor $\dot{V}_{pcc}(f)$ across a wide frequency spectrum.

2.2. Long Short-Term Memory (LSTM) Networks

Long Short-Term Memory (LSTM) networks are a specialized type of Recurrent Neural Network (RNN) designed to overcome the vanishing gradient problem, making them highly effective at learning long-term dependencies in sequential data [32]. This capability is essential for modeling the dynamic behavior of power systems, where the current state is influenced by a long history of past inputs.

The core innovation of the LSTM is its memory cell, which can maintain information over extended time intervals. The flow of information into and out of this cell is regulated by three sophisticated gates: the input gate (i_t), the forget gate (f_t), and the output gate (o_t). The structure of an LSTM cell is depicted in Figure 1.

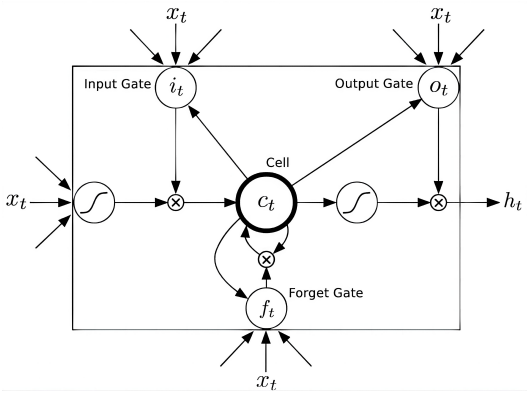


Figure 1. The core structure of a Long Short-Term Memory (LSTM) cell, illustrating the cell state (c_t) and the three regulatory gates.

At each time step t, given an input x_t and the previous hidden state h_{t-1}, the LSTM cell updates its internal cell state c_t and computes the output hidden state h_t. The key equations are:

$$f_t = \sigma(W_f x_t + U_f h_{t-1} + b_f) \quad (2)$$

$$i_t = \sigma(W_i x_t + U_i h_{t-1} + b_i) \quad (3)$$

$$o_t = \sigma(W_o x_t + U_o h_{t-1} + b_o) \quad (4)$$

$$\tilde{c}_t = \tanh(W_c x_t + U_c h_{t-1} + b_c) \quad (5)$$

$$c_t = f_t \odot c_{t-1} + i_t \odot \tilde{c}_t \quad (6)$$

$$h_t = o_t \odot \tanh(c_t) \quad (7)$$

where W, U are weight matrices, b are bias vectors, $\sigma(\cdot)$ is the sigmoid function, and $\odot$ denotes the element-wise product. The forget gate determines what information to discard from the cell state, the input gate decides what new information to store, and the output gate controls what information is passed on to the next hidden state. For this work, a Bidirectional LSTM (Bi-LSTM) network is employed, which processes the input sequence in both forward and backward directions, allowing the model to leverage both past and future context for every time step.

2.3. Problem Formulation

The primary objective of this paper is to develop a robust, data-driven model that accurately represents the frequency-domain impedance of a wind turbine without access to its internal parameters. The model should be capable of predicting the three-phase current response at the PCC, $\mathbf{I}_{pcc}(t) = [I_a(t), I_b(t), I_c(t)]^T$, given the corresponding three-phase voltage, $\mathbf{V}_{pcc}(t) = [V_a(t), V_b(t), V_c(t)]^T$, and the ambient wind speed conditions, $\mathbf{v}_{wind}$.

Let the proposed modeling framework be represented by a mapping function $\mathcal{F}$. The problem can be formally stated as finding the optimal set of parameters θ^* for this function:

$$\hat{\mathbf{I}}_{pcc}(t) = \mathcal{F}(\mathbf{V}_{pcc}(t), \mathbf{v}_{wind}; \theta) \tag{8}$$

where $\hat{\mathbf{I}}_{pcc}(t)$ is the predicted current time series. The model is trained by minimizing a loss function, such as the Mean Squared Error (MSE), between the predicted current and the ground-truth current $\mathbf{I}_{pcc}(t)$ obtained from high-fidelity simulations:

$$\theta^* = \arg\min_{\theta} \mathbb{E}\left[||\mathbf{I}_{pcc}(t) - \hat{\mathbf{I}}_{pcc}(t)||^2\right] \tag{9}$$

Once the model is trained, the frequency-domain impedance, $\dot{Z}_{wt}(f)$, can be calculated by applying the Fast Fourier Transform (FFT) to the predicted time-domain waveforms for any given voltage perturbation, thus enabling comprehensive stability analysis. The challenge lies in designing the function $\mathcal{F}$ such that it is not only accurate but also physically consistent and generalizable across a wide range of operating frequencies and wind conditions.

3. Modeling Frameworks for Wind Turbine Impedance

This section presents a comprehensive development of two distinct modeling frameworks for identifying the impedance characteristics of a wind turbine. It begins by detailing a purely data-driven "black-box" model, which, while effective to a degree, serves as a crucial baseline to highlight the inherent limitations that motivate the primary contribution. Subsequently, an exhaustive description of the novel Physics-Informed Hybrid Model (PIHM) is provided, elucidating its architecture, parameterization, and learning algorithm in full detail.

3.1. Black-Box Modeling with a Pure Bi-LSTM Network

The black-box paradigm offers a pragmatic approach to modeling complex systems like wind turbines when internal parameters are inaccessible. This methodology relies entirely on input–output measurement data to train a model that can replicate the system's behavior.

3.1.1. Model Formulation and Architecture

The impedance modeling problem is formulated as a sequence-to-sequence learning task. The model, denoted as $\mathcal{F}_{BB}$, is designed to learn the direct mapping from the observable inputs—the three-phase PCC voltage time series, $\mathbf{V}_{pcc}(t) \in \mathbb{R}^{T\times 3}$, and the cor-

responding quasi-static wind speed vector, $\mathbf{v}_{wind} \in \mathbb{R}^3$—to the three-phase output current time series, $\hat{\mathbf{I}}_{pcc}(t) \in \mathbb{R}^{T\times 3}$. The mathematical representation is:

$$\hat{\mathbf{I}}_{pcc}(t) = \mathcal{F}_{BB}(\mathbf{V}_{pcc}(t), \mathbf{v}_{wind}; \theta_{bb}) \tag{10}$$

where T is the sequence length, and θ_{bb} represents the full set of trainable parameters of the neural network.

The network architecture is built around a Bi-LSTM core [33]. The input at each time step t is a feature vector $x_t \in \mathbb{R}^6$, formed by concatenating the instantaneous three-phase voltage values and the three equivalent wind speeds (which are held constant across the sequence). The Bi-LSTM processes the input sequence $X = [x_1, x_2, \ldots, x_T]$ to produce a sequence of hidden states $H = [h_1, h_2, \ldots, h_T]$. By processing the data in both forward and backward directions, the hidden state h_t at any time t encapsulates information from the entire sequence, making it well suited for dynamic system modeling [23]. A final multi-layer perceptron (MLP) acts as a regression head, mapping each hidden state h_t to the predicted three-phase current vector $\hat{\mathbf{I}}_{pcc}(t)$ for that instant, and the complete model is optimized end-to-end by minimizing the Mean Squared Error (MSE) between the predicted and the ground-truth current sequences.

3.1.2. Inherent Limitations

While this black-box model can achieve high fidelity on test data drawn from the same distribution as the training data, its practical application is hampered by several fundamental weaknesses:

- Lack of Physical Grounding: The model operates without any intrinsic knowledge of the underlying physics. It does not inherently respect fundamental electrical principles like Ohm's Law or Kirchhoff's Laws, which can lead to physically implausible predictions under novel conditions.
- Poor Generalization and Robustness: Its performance is critically dependent on the comprehensiveness of the training data. It may fail to generalize to different grid strengths, new types of disturbances, or operating points far from those seen during training.
- Interpretability Deficit: The learned weights within the deep neural network lack direct physical meaning, making the model an "unexplainable" black box. This erodes trust and makes it difficult to diagnose or verify its behavior.

These significant drawbacks motivate the development of a more sophisticated gray-box model.

3.2. The Proposed Physics-Informed Hybrid Model (PIHM)

To transcend the inherent limitations of the purely data-driven paradigm, the PIHM was conceived and developed. This gray-box framework integrates fundamental physical principles with the nonlinear function approximation capabilities of a deep neural network. The PIHM was engineered as a cohesive system that is accurate, robustly generalizable, and physically interpretable.

3.2.1. Conceptual Framework and Architectural Design

The foundational design choice of the PIHM is its parallel architecture, as depicted in Figure 2. The total current at the point of common coupling is modeled as the superposition of two components: (1) the current produced by a simplified physical impedance circuit and (2) the residual current predicted by the Bi-LSTM network. This superposition principle is directly analogous to Kirchhoff's Current Law and provides a physically grounded

constraint on the model output. This configuration was deliberately selected over a series or a more deeply integrated structure to enable a clear and effective division of labor. A series architecture, where the neural network might correct the output of a physical model, can lead to error propagation. A fully integrated model, where physical laws act only as soft constraints in the loss function (a typical PINN approach), may not sufficiently enforce physical behavior. The parallel structure, however, models the total system current as a direct superposition of currents from two distinct branches, a principle directly analogous to Kirchhoff's Current Law.

As shown in Figure 2, the model receives three-phase PCC voltage $\mathbf{V}_{pcc}$ and wind speed $\mathbf{v}_{wind}$ as inputs. The physical branch (parameterized by Z_s and Z_p) computes the physics-based current component $\mathbf{I}_p$ using discretized IIR filters. Concurrently, the Bi-LSTM receives the internal node voltage $\mathbf{V}_{in}$—derived by subtracting the voltage drop across the series branch from $\mathbf{V}_{pcc}$—and produces the residual current $\mathbf{I}_{nn}$. The two branches are coupled at $\mathbf{V}_{in}$, resolved through an iterative inner loop (see Algorithm 1). The final output is $\mathbf{I}_{out} = \mathbf{I}_p + \mathbf{I}_{nn}$.

Algorithm 1 Training and inference algorithm for the PIHM framework.

Input: Time-series data $\{\mathbf{V}_{pcc}, \mathbf{v}_{wind}, \mathbf{I}_{true}\}$, number of iterations K.
Offline Step: Determine optimal fixed parameters for Z_s and Z_p using the constrained phase-error minimization method.
Initialization: Initialize Bi-LSTM parameters θ_{nn} with a specific scheme (e.g., Xavier).

function FORWARDPASS($\mathbf{V}_{pcc}, \mathbf{v}_{wind}, \theta_{nn}$)
    Initialize internal voltage: $\mathbf{V}_{in}^{(0)} \leftarrow \mathbf{V}_{pcc}$
    for $k = 1$ to K **do**
        Predict NN current: $\mathbf{I}_{nn}^{(k)} \leftarrow \mathcal{F}_{nn}(\mathbf{V}_{in}^{(k-1)}, \mathbf{v}_{wind}; \theta_{nn})$
        Calculate parallel branch current via discretized filter: $\mathbf{I}_p^{(k)} \leftarrow \text{apply_filter}(Z_p, \mathbf{V}_{in}^{(k-1)})$
        Calculate total output current: $\mathbf{I}_{out}^{(k)} \leftarrow \mathbf{I}_{nn}^{(k)} + \mathbf{I}_p^{(k)}$
        Update internal voltage: $\mathbf{V}_{in}^{(k)} \leftarrow \mathbf{V}_{pcc} - \text{apply_filter}(Z_s, \mathbf{I}_{out}^{(k)})$
    end for
    return $\mathbf{I}_{out}^{(K)}$
end function

procedure TRAINMODEL
    for each training epoch **do**
        for each batch in training data **do**
            $\hat{\mathbf{I}}_{out} \leftarrow \text{ForwardPass}(\mathbf{V}_{pcc}, \mathbf{v}_{wind}, \theta_{nn})$
            Calculate loss: $\mathcal{L} = \text{MSE}(\hat{\mathbf{I}}_{out}, \mathbf{I}_{true})$
            Backpropagate gradients $\nabla_{\theta_{nn}}\mathcal{L}$ through the iterative process.
            Update θ_{nn} using Adam optimizer and learning rate scheduler.
        end for
    end for
end procedure

This design choice provides several key advantages. First, it guarantees that a portion of the model's output is always governed by a well-defined, interpretable physical law, thereby grounding the entire model in physical reality. Second, it creates a residual learning problem for the neural network, which has been shown to be more effective and efficient than learning a full mapping from scratch [34]. Third, it provides a natural mechanism for model analysis, allowing inspection of the contributions of the physical and neural components separately. The entire system is coupled through a dynamic internal node

voltage, $\mathbf{V}_{in}(t)$, which represents a physically meaningful, albeit unmeasured, state within the system, creating a realistic closed-loop representation.

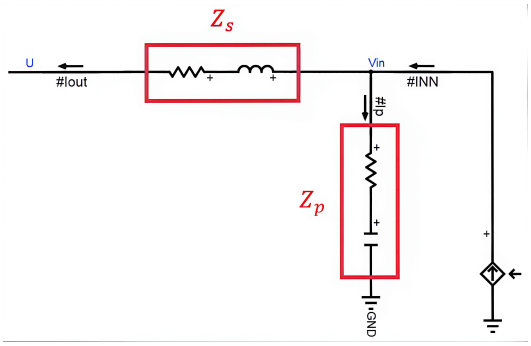


Figure 2. The proposed Physics-Informed Hybrid Model (PIHM) architecture. The model operates in two parallel branches: (1) a physical branch consisting of a series RL impedance Z_s and a parallel RC admittance Z_p, which produces the physics-based current $\mathbf{I}_p$; (2) a Bi-LSTM network that receives the internal node voltage $\mathbf{V}_{in}$ and predicts the residual current $\mathbf{I}_{nn}$. Both branches are coupled at the dynamic internal node $\mathbf{V}_{in}$, and the total output current is $\mathbf{I}_{out} = \mathbf{I}_p + \mathbf{I}_{nn}$. The # symbol labels the branch currents in the figure.

3.2.2. Physical-Branch Formulation and Discretization

The physical branch is intentionally designed as a simplified linear time-invariant (LTI) system. It is not intended to be a complete model of the high-order wind turbine. Instead, its purpose is to capture the baseline, dominant impedance characteristics, such as the effects of filters and transformers. This deliberate under-approximation is central to the decoupled learning strategy. By modeling the fundamental linear response, the physical branch simplifies the learning task for the neural network, which can then dedicate its full capacity to modeling the remaining complex, high-order, and nonlinear dynamics that the LTI model cannot capture. This synergy is the key to the framework's effectiveness.

This includes the aggregate effects of the main transformer, cabling, and the converter's passive filter components. It consists of two carefully chosen sub-components:

- A series RL impedance, Z_s: This component models the series impedance elements connecting the internal converter voltage source to the PCC. Its impedance, $Z_s(s) = R_s + sL_s$, where s is the complex frequency variable of the Laplace transform, primarily represents the resistive losses and leakage inductance of transformers and transmission lines. This is a standard and effective representation for such elements in power system analysis [35].
- A parallel RC admittance, Y_p: This component models the dominant shunt characteristics of the system. The parallel combination of a resistor R_p and a capacitor C_p creates an admittance $Y_p(s) = 1/R_p + sC_p$, which corresponds to an equivalent impedance $Z_p(s) = 1/Y_p(s) = R_p/(1 + sR_pC_p)$. This structure serves a dual purpose: the capacitance models the low-pass filtering effect inherent in the converter's DC-link and AC-side filters, while the resistance represents the system's damping properties or an equivalent load [36].

The time-domain behavior of this physical branch is described by a set of ordinary differential equations (ODEs). The current through the parallel branch, $\mathbf{I}_p(t)$, driven by the internal node voltage $\mathbf{V}_{in}(t)$, is:

$$\mathbf{I}_p(t) = \frac{1}{R_p}\mathbf{V}_{in}(t) + C_p\frac{d\mathbf{V}_{in}(t)}{dt} \tag{11}$$

The relationship defining the internal node voltage based on the PCC voltage and the total output current, $\mathbf{I}_{out}(t)$, flowing through the series branch is:

$$\mathbf{V}_{in}(t) = \mathbf{V}_{pcc}(t) - \left(R_s \mathbf{I}_{out}(t) + L_s \frac{d\mathbf{I}_{out}(t)}{dt} \right) \tag{12}$$

For implementation within the discrete-time algorithm, these continuous ODEs must be discretized. The bilinear transform is employed (Tustin's method with pre-warping) to convert the continuous transfer functions $Z_s(s)$ and $Y_p(s)$ into discrete IIR (Infinite Impulse Response) filters. This method is chosen for its property of mapping the left-half of the s-plane to the interior of the unit circle in the z-plane, thus preserving the stability of the original LTI system. This discretization step is a critical detail for the practical implementation and stable simulation of the physical branch within the iterative forward pass of the model.

3.2.3. Parameter Identification via Constrained Phase-Error Minimization

A pivotal and labor-intensive part of the work is the development of a systematic, data-driven methodology for identifying the optimal parameters (R_s, L_s, R_p, C_p) for the physical branch. This procedure is essential as it makes the framework independent of proprietary manufacturer data. The method is a constrained optimization process based on the insight that the phase angle of the impedance is a highly sensitive and critical indicator of a system's dynamic performance and stability margins.

The offline procedure involves an exhaustive grid search over a wide, physically plausible parameter space [37]. For each point on this multi-dimensional grid, the following evaluation is performed:

1. For a batch of representative voltage signals $\mathbf{V}_{pcc}(t)$ from the training set, calculate the theoretical current response $\mathbf{I}_{cand}(t)$ that would be produced by the candidate physical impedance.
2. Using the Fast Fourier Transform (FFT), extract the phasors of both the candidate current ($\dot{I}_{cand}$) and the ground-truth current ($\dot{I}_{true}$) at the fundamental grid frequency (50 Hz).
3. Compute two crucial metrics: the magnitude ratio, $\rho = |\dot{I}_{cand}|/|\dot{I}_{true}|$, and the phase error, $\Delta\phi = |\angle\dot{I}_{true} - \angle\dot{I}_{cand}|$. Phase angle is used as the primary optimization criterion because it is a sensitive indicator of a system's dynamic behavior and stability margins in impedance-based analysis [31].
4. The final optimization is constrained. First, filter the parameter grid to include only those points that satisfy the magnitude constraint $\rho < \alpha$ (where $\alpha = 0.8$ was determined through cross-validation on the training set to ensure a meaningful residual remains for the neural network). This constraint is critical; it ensures the physical branch is a deliberate under-approximation of the true system, guaranteeing that a significant, learnable residual dynamic remains for the neural network [38].
5. From this valid, constrained set of parameters, select the one that minimizes the average phase error $\Delta\phi$ across all test samples.

Figure 3 visualizes the current-ratio constraint, the phase-error landscape, and the resulting phase-error distribution over the valid parameter set. This transparent, justifiable, and data-driven parameterization makes the gray-box framework robust, reproducible, and practically applicable.

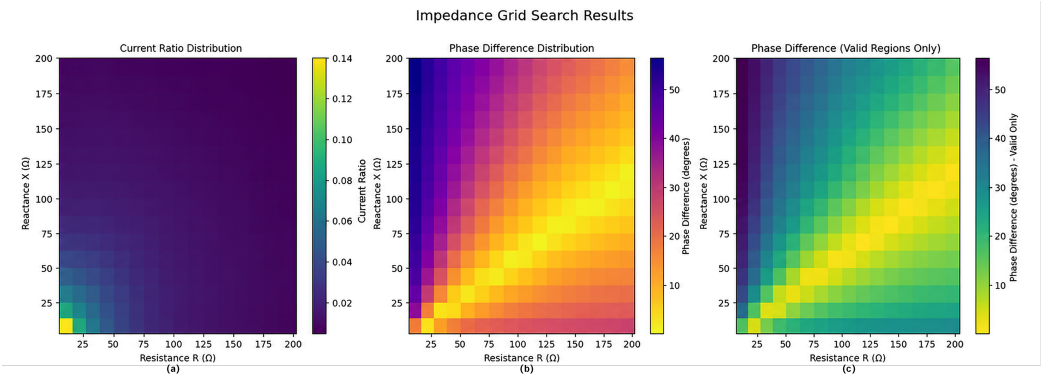


Figure 3. Grid search visualization for optimal parallel branch parameters. (**a**) Heatmap of the current magnitude ratio (ρ). (**b**) Heatmap of the phase error ($\Delta\phi$). (**c**) Phase error within the valid region satisfying the magnitude constraint, with the optimal point (minimal error) marked.

3.2.4. Bi-LSTM Architecture and Decoupled Learning Strategy

With the physical branch parameters identified and held constant, the training process focuses exclusively on optimizing the parameters of the Bi-LSTM network. This network is specifically structured to handle the residual modeling task. The core of the network consists of two stacked Bi-LSTM layers, each with a hidden state dimension of 256. This depth provides sufficient capacity to learn complex temporal patterns. To combat overfitting, a common challenge in deep learning, a Dropout layer with a rate of 0.3 is strategically placed after the Bi-LSTM layers. The output sequence from the Dropout layer is then processed by a time-distributed multi-layer perceptron (MLP) head. This head consists of two fully connected layers with a LeakyReLU activation function, which helps mitigate the vanishing gradient problem and allows for a more effective training of deep architectures.

The synergy between the fixed physical branch and the trainable neural network enables an effective decoupled learning strategy. The Bi-LSTM is not burdened with learning the entire system response from first principles. The learning target for the neural network is effectively transformed into the residual current $\mathbf{I}_{residual}(t) = \mathbf{I}_{true}(t) - \mathbf{I}_p(t)$. This residual signal typically contains higher-frequency components and nonlinearities that are difficult to capture with a simple linear model but are an ideal learning target for a dynamic neural network like an LSTM. This offloading of the "easy" linear dynamics to an interpretable physical model allows the deep learning component to dedicate its full expressive power to the most challenging parts of the problem, leading to faster convergence, better final accuracy, and a more robust overall model.

3.2.5. Iterative Solution Algorithm and Advanced Training

A unique feature of the PIHM's architecture is the closed-loop dependency between the internal node voltage $\mathbf{V}_{in}$ and the total output current $\mathbf{I}_{out}$. This is captured by the relationship from Equation (12), which in the Laplace domain is:

$$\dot{V}_{in}(s) = \dot{V}_{pcc}(s) - \dot{I}_{out}(s)Z_s(s) \tag{13}$$

This circular dependency cannot be resolved in a single step. Therefore, an iterative solution scheme within each forward pass of the model is implemented, as formalized in Algorithm 1. For a small, fixed number of iterations K (empirically set to $K = 3$ for a good balance of accuracy and computational cost), the model repeatedly updates its estimates of the internal state variables. In each sub-iteration, the neural network produces a new estimate of $\mathbf{I}_{nn}$, which is combined with the physical current $\mathbf{I}_p$ to update the total current $\mathbf{I}_{out}$. This new total current is then used to update the internal voltage $\mathbf{V}_{in}$, which becomes the input for the next sub-iteration. This "relaxation-style" process allows the physical

and neural components to dynamically interact and converge to a mutually consistent equilibrium state for each time step in the sequence.

The entire framework is trained end-to-end using the Adam optimizer [39], which is well suited for training large neural networks. The loss function is the standard Mean Squared Error (MSE). To ensure robust convergence and avoid getting trapped in poor local minima, an advanced learning rate scheduling strategy is employed: Cosine Annealing with Warm Restarts. This schedule cyclically varies the learning rate between a high and a low value, which helps the optimizer to explore the loss landscape more effectively. The training is monitored, and early stopping is used to prevent overfitting and select the model with the best performance on a validation set.

4. Case Study and Results Analysis

This section presents a comprehensive empirical evaluation of the proposed PIHM. A series of case studies were conducted using a high-fidelity simulation environment to validate the model's performance. The primary objectives were: (1) to conduct a rigorous ablation study by comparing the PIHM against a purely data-driven baseline to prove the efficacy of the hybrid architecture; (2) to assess the model's absolute accuracy in both time and frequency domains; and (3) to demonstrate its robustness and generalization capability under a wide range of operating conditions.

4.1. Simulation Setup and Dataset Generation

To ensure the reproducibility and validity of the results, a detailed and controlled experimental environment was established.

4.1.1. Simulation Platform and System Model

The "ground-truth" data for this study were generated using the CloudPSS simulation platform, a state-of-the-art tool for power system electromagnetic transient simulations. The system under study, depicted in Figure 4, is a representative model of a modern wind farm connected to the grid. It consists of three 2 MW DFIG units, aggregated into a single equivalent model for computational efficiency, connected to the main grid through a step-up transformer and transmission line. This detailed model captures the complex, nonlinear dynamics of the turbine's control systems, providing a realistic data source for training and validation.

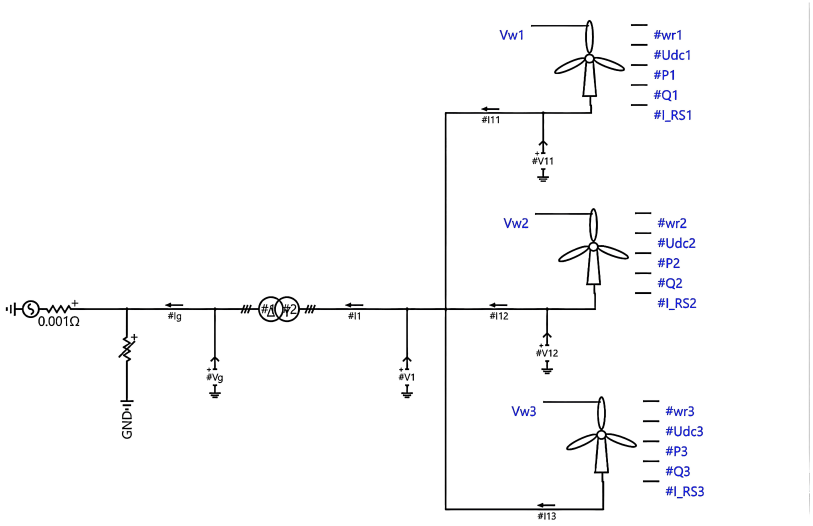


Figure 4. The equivalent circuit model of the grid-connected DFIG wind farm used in the CloudPSS simulation platform to generate the ground-truth data. The # symbol labels the branch currents and nodal voltages in the figure.

4.1.2. Dataset Generation

A comprehensive dataset was systematically generated to train and evaluate the models. To capture the turbine's frequency-domain characteristics, a frequency sweep methodology was employed. A small-signal sinusoidal voltage perturbation, with an amplitude of 3% of the nominal voltage, was superimposed onto the fundamental grid voltage. The frequency of this perturbation was swept across a wide band from 10 Hz to 1000 Hz. For each simulation, the system was run for 60 s, with the perturbation applied after an initial 15-s settling period to ensure the system started from a steady state. All voltage and current waveforms were recorded at a high sampling rate of 3000 Hz.

To evaluate the model's robustness and generalization, this process was repeated under four distinct wind speed scenarios:

- Uniform Low Speed: All three equivalent units operating randomly between 5.5 m/s and 6 m/s.
- Uniform Medium Speed: All units operating randomly between 8 m/s (considered the standard case) and 10.7 m/s.
- Uniform High Speed: All units operating randomly between 10.8 m/s and 13.8 m/s.
- Non-Uniform Speed: Units operating randomly at low, medium, and high speeds, respectively, to simulate unbalanced conditions.

The resulting dataset, comprising over 100 individual simulation runs, was partitioned into training (70%), validation (10%), and testing (20%) sets, ensuring no overlap between them.

4.1.3. Model Implementation and Evaluation Metrics

Both the proposed PIHM and the baseline Pure Bi-LSTM model were implemented in Python 3.8 using the PyTorch 2.1.2 deep learning framework. The specific hyperparameters and training configurations, which were kept identical for both models to ensure a fair comparison, are summarized in Table 1. The physical parameters for the PIHM's impedance branches, identified using the phase-error minimization method, were found to be $R_s = 2\,\Omega$, $L_s = 0.3$ mH, $R_p = 30\,\Omega$, $C_p = 100\,\mu$F.

Table 1. Hyperparameter and training configuration.

Parameter	Value
Bi-LSTM Hidden Dimension	256
Number of Bi-LSTM Layers	2
Dropout Rate	0.3
Optimizer	Adam
Initial Learning Rate	1×10^{-4}
Learning Rate Scheduler	Cosine Annealing with Warm Restarts
Batch Size	128
Max Epochs	200 (with early stopping)
PIHM Iterations (K)	3

Model performance was evaluated using both time-domain and frequency-domain metrics. In the time domain, the Coefficient of Determination (R^2) and Mean Squared Error (MSE) on the predicted current waveforms were used. In the frequency domain, a qualitative and quantitative comparison of the impedance magnitude (in dB) and phase (in degrees) plots against the ground truth was performed.

4.2. Model Accuracy and Performance Evaluation

After establishing the experimental setup, this section first evaluates the absolute accuracy of the proposed PIHM. The objective is to demonstrate its capability to perform its primary function: predicting the system's electrical response with high fidelity in both the time and frequency domains under standard operating conditions (8 m/s wind speed).

4.2.1. Time-Domain Current Prediction

The model's direct output was a time-domain current waveform, the accuracy of which was fundamental to all subsequent analysis. The quantitative performance on the unseen test set, summarized in Table 2, was excellent. The Mean Squared Error was exceptionally low, and the Coefficient of Determination (R^2) across all three phases was consistently above 0.98, indicating that the model explained over 98% of the variance in the true data.

To further illustrate this high degree of correlation, Figure 5 presents scatter plots of the predicted current versus the actual current for each phase. The data points cluster tightly around the ideal y = x line, visually confirming the high R^2 values and the model's unbiased predictive power. For a qualitative view, Figure 6 shows a snapshot from the test set. The predicted waveforms (dashed lines) are visually almost indistinguishable from the ground-truth waveforms (solid lines), tracking both the amplitude and phase of the three-phase currents with high fidelity. The combination of high scores on quantitative metrics and the near-perfect visual overlap confirms that the PIHM functions as a high-fidelity simulator of the turbine's terminal electrical behavior. This foundational accuracy is the essential prerequisite for reliable impedance calculation.

Table 2. Time-domain performance metrics of PIHM on test set.

Metric	Value
Mean Squared Error (MSE)	1.24×10^{-4}
Average R-Squared (R^2)	0.9894
Phase A R^2	0.9877
Phase B R^2	0.9892
Phase C R^2	0.9914

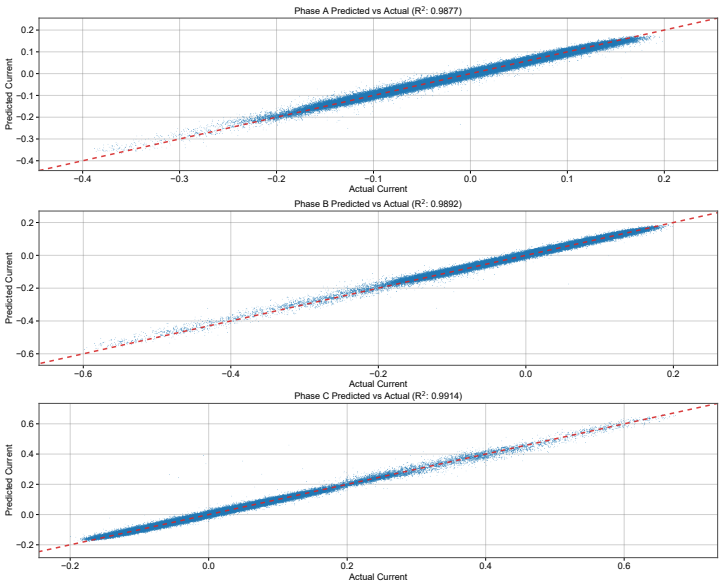


Figure 5. Scatter plots of predicted vs. actual current for each phase, demonstrating the high correlation and R-squared values reported in Table 2.

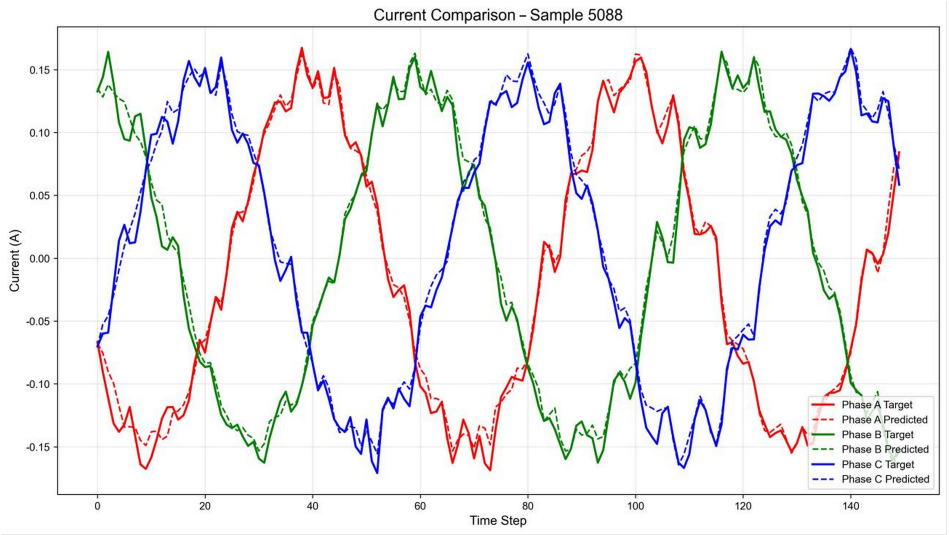


Figure 6. Time-domain current prediction for a sample from the test set. The predicted three-phase currents (dashed lines) show excellent agreement with the ground-truth waveforms (solid lines).

4.2.2. Frequency-Domain Impedance Accuracy

The ultimate utility of the model lies in its application to frequency-domain stability analysis. The PIHM predicts the current for each of the three phases individually. Figure 7 shows the impedance profiles calculated for each phase, along with their mathematical average. The close alignment of the curves for Phase A, B, and C demonstrates that the model has learned a well-balanced representation and is not biased towards any single phase. The averaged result is a stable and clean representation of the overall system impedance that can be used for all subsequent analysis.

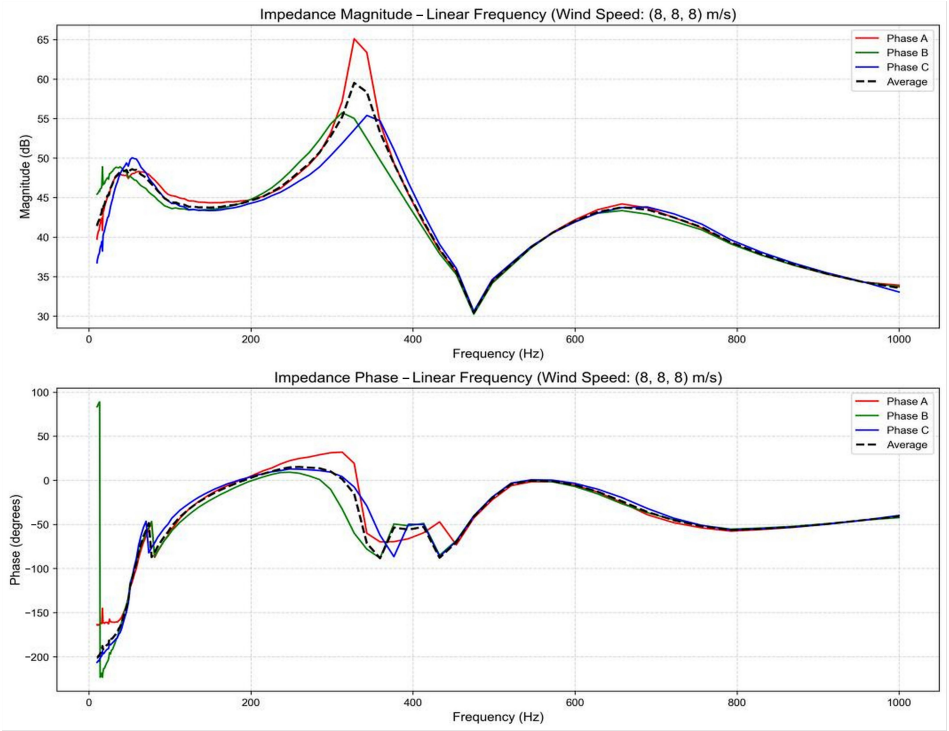


Figure 7. Impedance profiles for each individual phase and their average, as predicted by the PIHM for the 8 m/s case. The consistency across phases confirms a balanced model.

The averaged impedance profile provides a stable representation for frequency-domain stability analysis. It preserves the key resonant and anti-resonant characteristics observed

in the high-fidelity simulation and maintains phase consistency around the dominant dynamic transitions. This behavior confirms that the PIHM learns the system's wide-band dynamic response in a physically meaningful form, which is essential for identifying potential subsynchronous oscillation risks.

4.3. Ablation Study: The Value of the Physics-Informed Architecture

The ablation study was designed to examine how the physics-informed hybrid architecture changed the behavior of a standard black-box baseline. To isolate the role of the physical branch and the decoupled residual-learning strategy, the PIHM was compared against its purely data-driven counterpart, a Pure Bi-LSTM model, under the standard 8 m/s wind speed test case.

Table 3 presents a quantitative comparison of the two models in both the time and frequency domains. The time-domain entries were computed from the saved test-set predictions and show that the two models have comparable waveform accuracy. The frequency-domain entries were computed on 149 stable points of the 8 m/s CloudPSS impedance sweep using the finalized evaluation protocol. Under this protocol, the PIHM still has lower magnitude and phase MAE than the Pure Bi-LSTM baseline.

Table 3. Quantitative comparison: PIHM vs. Pure Bi-LSTM (8 m/s test case).

Model	R^2	MSE	$\mathbf{MAE_{mag}}$ (dB)	$\mathbf{MAE_{phase}}$ (°)
Pure Bi-LSTM	0.9865	9.87×10^{-5}	10.377	24.349
PIHM (proposed)	0.9894	1.24×10^{-4}	2.548	15.183

The ablation study reveals a clear difference in behavior between the two modeling strategies. The ground-truth impedance derived from high-fidelity transient simulation naturally contains high-frequency fluctuations caused by the complex switched-converter dynamics. A purely data-driven Bi-LSTM tends to chase these fluctuations, which leads to less stable and less physically plausible impedance estimates, particularly in the high-frequency phase response. In contrast, the PIHM uses its physical branch as a structured baseline and assigns the neural network to the residual dynamics, yielding smoother and more physically consistent impedance profiles.

These observations support the value of the hybrid framework and the decoupled learning strategy. Embedding even a simplified physical model acts as a regularizer that constrains the solution toward plausible electrical behavior. The physical branch handles the baseline linear response, while the Bi-LSTM focuses on the more compact residual-learning problem. This decomposition improves robustness and reduces the risk that the model will confuse numerical or switching artifacts with the true dynamic impedance trend.

4.4. Robustness and Generalization to Varying Wind Conditions

For a model to be practically useful, it must be robust against variations in operating conditions. This experiment was designed as a stress test to evaluate the model's generalization capability. The single, already-trained PIHM was evaluated on entirely unseen test sets corresponding to different wind speeds, which significantly altered the turbine's operating point and dynamic response.

The results of this test are presented in two complementary ways. First, Figure 8 provides a high-level comparison by overlaying the impedance profiles predicted by the single PIHM model for four different wind scenarios. The model remains stable and produces smooth, physically consistent impedance curves across all scenarios. Critically, it correctly captures a key physical trend: as the wind speed increases, the active power

injection from the turbine increases, which generally leads to a lower overall impedance magnitude. This is clearly visible as the curves shift downwards from the 6 m/s case (green) to the 12 m/s case (purple).

To further scrutinize the model's performance under each specific condition, Figure 9 presents the individual comparisons against their respective ground truths. The plots for magnitude (Figure 9a) and phase (Figure 9b) show strong agreement across all tested conditions. Even under the challenging non-uniform case, which represents an unbalanced operating condition, the model produces a coherent and stable average impedance profile that closely matches the ground truth.

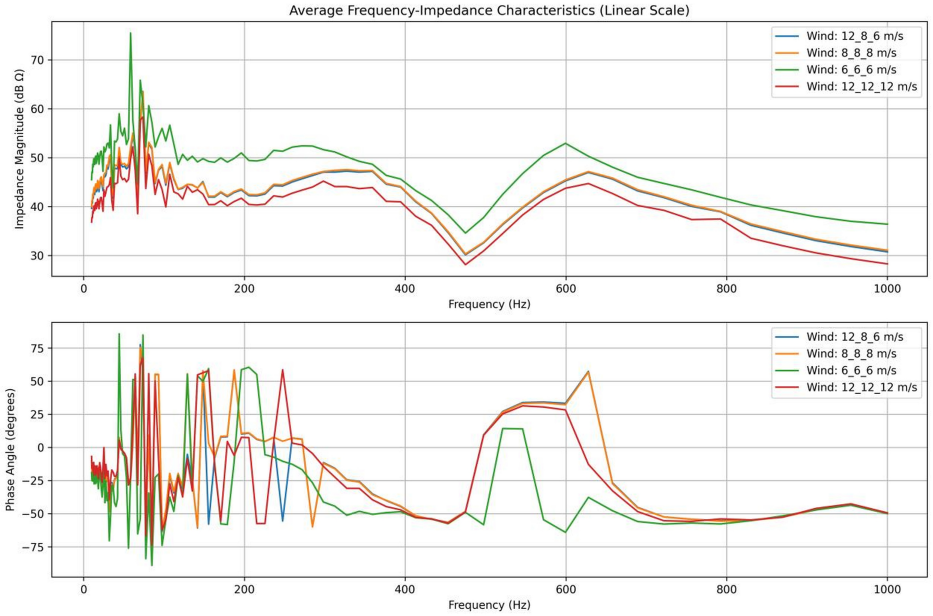


Figure 8. Predicted impedance profiles from the single trained PIHM under four different wind speed scenarios: uniform 6 m/s, 8 m/s, 12 m/s, and a non-uniform case.

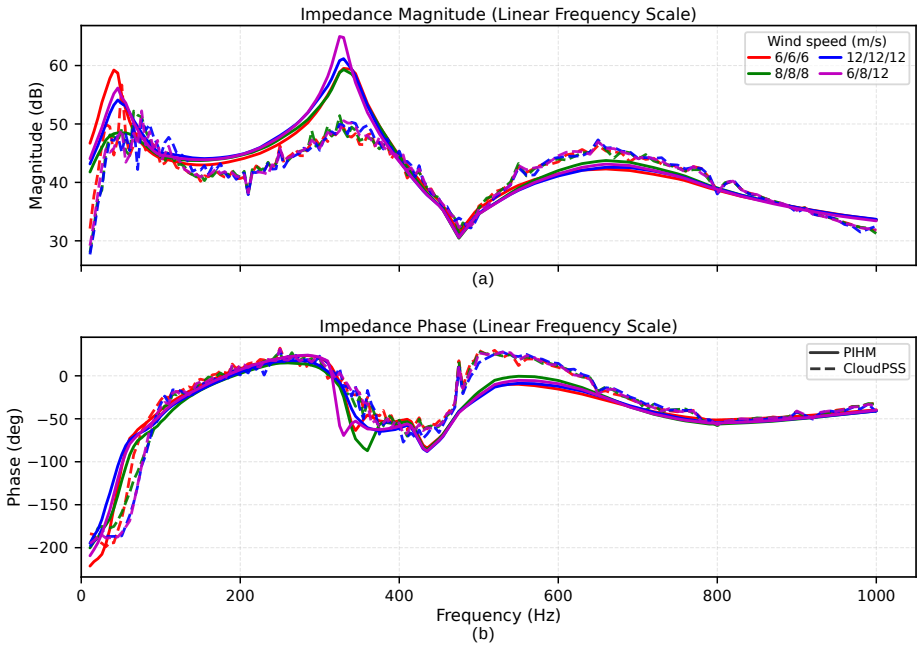


Figure 9. Individual impedance profiles for various wind conditions, comparing the single trained PIHM prediction (solid lines) with the corresponding CloudPSS ground-truth impedance curves (dashed lines).

These results demonstrate the generalization capability of the PIHM, supporting the value of the systematic parameter identification method. The systematically identified physical branch provides a robust and stable "anchor" for the model. Because this anchor is grounded in physics, it behaves predictably across different operating points. The neural network, having learned the residual dynamics, is able to adapt this residual smoothly on top of the stable physical baseline. This is a significant advantage over a purely black-box model, which, lacking this physical anchor, is more likely to exhibit degraded performance when faced with diverse operating conditions not well represented in the training data. This demonstrates that the PIHM is not only accurate but also robust and generalizable across varying operating conditions.

4.5. Discussion of Results

The experimental results provide strong support for the proposed PIHM framework across a multi-faceted evaluation. The findings from each case study directly map to the core contributions of this paper.

The quantitative accuracy of the PIHM ($R^2 = 0.9894$, MSE $= 1.24 \times 10^{-4}$) confirms that the framework achieves high-fidelity time-domain current prediction, which is the prerequisite for reliable frequency-domain impedance extraction. The near-perfect alignment of the predicted and ground-truth waveforms across all three phases (Phase A: $R^2 = 0.9877$; Phase B: $R^2 = 0.9892$; Phase C: $R^2 = 0.9914$) also confirms that the model does not introduce any phase-specific bias.

First, the role of the hybrid physics-informed framework was examined in the ablation study in Section 4.3. Although the two models had comparable time-domain waveform accuracy, the PIHM produced lower frequency-domain magnitude and phase errors under the finalized evaluation protocol. This contrast highlights the role of the physical branch as a regularizer that helps prevent the model from learning spurious impedance dynamics from the data.

Second, the efficacy of the decoupled learning strategy is substantiated by the high accuracy shown in both the ablation study (Section 4.3) and the performance evaluation (Section 4.3). By offloading the task of modeling the baseline linear response to the physical branch, the Bi-LSTM network focuses its capacity on the more complex, nonlinear residual dynamics. This simplified learning task leads to faster convergence, higher fidelity in both time and frequency domains, and a more stable final model.

Finally, the value of the systematic parameter identification method and the resulting model robustness was established in Section 4.4. The phase-error minimization technique provided a reproducible method for creating a stable physical "anchor" for the model. The generalization capability of a single trained PIHM across four distinct, unseen wind speed conditions—including the challenging non-uniform case—proved that this physical anchor enables the model to adapt predictably across different operating points.

It should be noted that the current validation was conducted exclusively on a DFIG simulation model under varying wind speed conditions. While the results are encouraging, the framework's behavior under other operating conditions—such as different short-circuit ratios (grid strength) or fault scenarios—was not explicitly evaluated in this work. These remain important open questions for future research. Furthermore, the validation on real-world measurement data from SCADA or PMU systems would be a necessary step before deployment. These limitations are acknowledged and form the basis of the future work outlined in the conclusion.

A further limitation concerns the frequency-domain generalization of the trained model. As Figure 9 illustrates, while the single trained model exhibits a degree of adaptability under the four wind speed scenarios, the agreement with the CloudPSS ground-truth

impedance is not uniform across the full 10–1000 Hz sweep; discrepancies are more pronounced at certain frequency sub-bands. This indicates that full generalization of the frequency-domain impedance characteristics from a time-domain-trained model remains an open challenge, and incorporating frequency-domain loss terms—such as a penalty on the impedance magnitude or phase error—into the training objective is a promising direction for future research.

In summary, the results confirm that the PIHM successfully integrates the strengths of both physics-based and data-driven approaches, achieving high accuracy while retaining physical interpretability and robustness.

5. Conclusions

This paper addressed the problem of wind turbine impedance modeling in the absence of proprietary manufacturer parameters, a practically important challenge for impedance-based stability analysis of modern wind power systems. A Physics-Informed Hybrid Model (PIHM) was proposed and validated, combining a simplified physical impedance branch with a Bi-LSTM network in a parallel gray-box architecture.

The key findings of this study are as follows. First, the parallel hybrid architecture, which assigns the dominant linear dynamics to the physical branch and the nonlinear residuals to the Bi-LSTM, yielded a high-fidelity current predictor with an average $R^2 = 0.989$ and MSE $= 1.24 \times 10^{-4}$ on the held-out test set, corresponding to smooth and physically consistent frequency-domain impedance profiles. Second, the ablation study confirmed that the physics-informed structure outperforms a purely data-driven Bi-LSTM baseline by suppressing unphysical high-frequency artifacts in the impedance estimates; the quantitative comparison is summarized in Table 3. Third, a single trained PIHM generalized successfully to four distinct wind speed conditions—uniform low (6 m/s), medium (8 m/s), high (12 m/s), and non-uniform—demonstrating the stabilizing role of the physically grounded branch.

Despite these results, several limitations motivate future work. (1) Validation with other generator types: The current study uses a DFIG model. Extending validation to Permanent-Magnet Synchronous Generator (PMSG) wind turbines is an important next step to assess the framework's generality. (2) Additional operating conditions: The generalization capability was tested only under wind speed variations. Evaluating the model under different grid strengths (short-circuit ratios) and fault conditions is necessary for a comprehensive assessment. (3) Field data validation: Replacing the simulation-generated training data with real-world measurements from SCADA or PMU systems would be required before practical deployment. (4) Online adaptation: Developing an online mechanism to update the physical branch parameters in response to long-term operating-point shifts would further improve the model's dynamic tracking capability. (5) Multi-turbine and multi-farm extension: Extending the modeling framework to capture the coupled impedance dynamics of multiple interconnected wind farms is an important direction for regional stability analysis.

The proposed PIHM provides a reliable, parameter-free baseline for impedance-based stability studies and establishes a gray-box design principle that can be adapted to other converter-interfaced generation technologies.

Author Contributions: Conceptualization, L.W. and T.X.; methodology, L.W., H.H., and Y.C.; software, J.X.; validation, J.X., H.H. and Y.C.; formal analysis, J.X.; investigation, T.X.; resources, L.W.; data curation, H.H.; writing—original draft preparation, L.W.; writing—review and editing, J.X., H.H., Y.C. and T.X.; visualization, T.X.; supervision, T.X.; funding acquisition, L.W. and T.X. All authors have read and agreed to the published version of the manuscript.

Funding: This paper was supported by the Science and Technology Project of China Southern Power Grid Co., Ltd. (Project No.: GXKJXM20222192).

Institutional Review Board Statement: Not applicable.

Informed Consent Statement: Not applicable.

Data Availability Statement: The data supporting the findings of this study are available from the corresponding author upon reasonable request.

Acknowledgments: The authors would like to thank Lifu Ding, Associate Professor at Zhejiang University, for his valuable contributions to the early stages of this work. This manuscript used Claude Sonnet 4.5 for language editing and writing improvement. The authors confirm that the model was not used to generate scientific content, interpret results, draw conclusions, or produce any original research findings presented in this manuscript.

Conflicts of Interest: Authors Libin Wen, Jinji Xi and Hong Hu were employed by the Electric Power Research Institute of Guangxi Power Grid Co., Ltd. The remaining authors declare that the research was conducted in the absence of any commercial or financial relationships that could be construed as a potential conflict of interest.

Abbreviations

The following abbreviations are used in this manuscript:

ANN	Artificial Neural Network
Bi-LSTM	Bidirectional Long Short-Term Memory
DFIG	Doubly Fed Induction Generator
FFT	Fast Fourier Transform
LTI	Linear Time-Invariant
MLP	Multi-Layer Perceptron
MSE	Mean Squared Error
PCC	Point of Common Coupling
PIHM	Physics-Informed Hybrid Model
PMU	Phasor Measurement Unit
RNN	Recurrent Neural Network
SCADA	Supervisory Control and Data Acquisition
SFRA	Sweep Frequency Response Analysis
SSO	Subsynchronous Oscillation
WT	Wind Turbine

References

1. Global Wind Energy Council. *Global Wind Report 2024*; GWEC: Brussels, Belgium, 2024.
2. Si, J.; Ai, L.; Qiu, C. Development status and prospect of wind power in China in 2023. *Water Power* **2024**, *50*, 1–4. 17.
3. Rehman, S.; Zayed, M.E.; Syed, A.H.; Ghazy, M.; Irshad, K.; Al-Shaikhi, A.; Mohandes, M.A.; Alhems, L.M. Assessment of offshore wind power potential in Saudi Arabia's Red Sea: Insights into fixed-bottom and floating offshore technologies. *Results Eng.* **2026**, *29*, 108626. [CrossRef]
4. Shboul, B.; Zayed, M.E.; Al-Tawalbeh, N.; Usman, M.; Irshad, K.; Odat, A.-S.; Alam, M.A.; Rehman, S. Dynamic Numerical Modeling and Performance Optimization of Solar and Wind Assisted Combined Heat and Power System Coupled with Battery Storage and Sophisticated Control Framework. *Results Eng.* **2024**, *22*, 102198. [CrossRef]
5. Erlich, I.; Shewarega, F.; Rueda, J.L. Impact of large offshore wind farms on power system transient stability. In Proceedings of the 2009 IEEE/PES Power Systems Conference and Exposition, Seattle, WA, USA, 15–18 March 2009; pp. 1–8.
6. Moradzadeh, M.; Shayeghi, H.; Vandevelde, L.; Saif, M. Impact of increased penetration of large-scale wind farms on power system dynamic stability—A review. In Proceedings of the 2015 IEEE 15th International Conference on Environment and Electrical Engineering (EEEIC), Rome, Italy, 10–13 June 2015; pp. 1522–1526.
7. Yang, B.; Xie, X.; Yan, G.; Zhan, Y. A review of subsynchronous oscillation analysis methods for grid-connected wind power systems. *Electr. Power Constr.* **2019**, *40*, 56–63.

8. Wang, Y.; Wang, X.; Liao, J.; Wang, H. A review on generation, identification and suppression of wide-band oscillations in AC/DC power grids. *High Volt. Eng.* **2023**, *49*, 3148–3162.
9. Zeng, Z.; Xiao, H.; Gao, B.; Wei, Z.; Wang, W.; Cheng, M. Analysis of harmonic resonance stability of grid-connected systems based on impedance ratio and oscillation damping characteristics. *Proc. CSEE* **2020**, *40*, 7201–7211.
10. Luo, K.; Guo, J.; Wang, W.; Wang, T.; Ma, S.; Wang, M.; Wang, G. Review of impacts of supplementary frequency control of grid-following renewable energy on frequency stability and small-signal synchronous stability. *Proc. CSEE* **2023**, *43*, 1262–1281.
11. Yang, L.; Zhu, Y.; Lin, S.; Luan, K.; Huang, W.; He, Y. Oscillation Suppressing Control Method Based on Impedance Optimization for Grid-Connected VSC-HVDC System. In Proceedings of the 2023 International Conference on Power System Technology (PowerCon), Jinan, China, 21–22 September 2023; pp. 1–7.
12. Li, X.; Fan, Y.; Hou, J.; Lu, J.; Xuan, D. Impedance modeling and small-signal stability analysis of DC Pooling wind power system. *High Volt. Eng.* **2025**, *51*, 1632–1644.
13. Mitra, A.; Chatterjee, D. Active Power Control of DFIG-Based Wind Farm for Improvement of Transient Stability of Power Systems. *IEEE Trans. Power Syst.* **2016**, *31*, 82–93. [CrossRef]
14. Giraldo, E.; Garces, A. An Adaptive Control Strategy for a Wind Energy Conversion System Based on PWM-CSC and PMSG. *IEEE Trans. Power Syst.* **2014**, *29*, 1446–1453.
15. Yin, M.; Li, G.; Zhang, J.; Zhao, W.; Xue, Y. Modeling and control strategies of direct driven wind turbine with permanent magnet synchronous generator. *Power Syst. Technol.* **2007**, *31*, 61–65.
16. Zhang, X.; Zhang, L.; Yang, S.; Yu, Y.; Cao, R. Low Voltage Ride-through Technologies in Wind Turbine Generation. *Proc. CSU-EPSA* **2008**, *20*, 1–8.
17. Chi, Y.; Wang, W.; Dai, H. Research on transient voltage stability of grid-connected wind farm based on doubly-fed induction generator. *Proc. CSEE* **2007**, *27*, 25–31.
18. He, J.; Luo, G.; Cheng, M.; Liu, Y.; Tan, Y.; Li, M. Review of new-generation artificial intelligence in power system fault analysis and location. *Proc. CSEE* **2020**, *40*, 5506–5515.
19. Long, H.; Yang, T.; Xu, S.; Gu, W. Review of data-driven condition monitoring and fault diagnosis technologies for wind turbines. *Autom. Electr. Power Syst.* **2023**, *47*, 55–69.
20. Liu, Y.; Yang, F.; Zhang, F.; Zhu, Y.; Ji, S.; Sun, X.; Fu, C. Study on sweep frequency Impedance to detect winding deformation within power transformer. *Proc. CSEE* **2015**, *35*, 4505–4516.
21. Chen, M.; Challita, U.; Saad, W. Artificial Neural Networks-Based Machine Learning for Wireless Networks: A Tutorial. *IEEE Commun. Surv. Tutor.* **2019**, *21*, 3039–3071. [CrossRef]
22. Alpaydin, E. *Introduction to Machine Learning*; MIT Press: Cambridge, MA, USA, 2014.
23. Zhang, H.; Zhao, L.; Du, Z. Wind power prediction based on CNN-LSTM. In Proceedings of the 2021 IEEE 5th Conference on Energy Internet and Energy System Integration (EI2), Taiyuan, China, 22–24 October 2021; pp. 3097–3102.
24. Zhu, Q.; Li, H.; Wang, Z.; Chen, J.; Wang, B. Short-term wind power forecasting based on LSTM. *Power Syst. Technol.* **2017**, *41*, 3797–3802.
25. Joudaki, M. Long-term wind speed and power forecasting based on LSTM: A comprehensive study. In Proceedings of the 2022 9th Iranian Conference on Renewable Energy & Distributed Generation (ICREDG), Mashhad, Iran, 23–24 February 2022; pp. 1–4.
26. Qian, P.; Ma, X.; Zhang, D. Data-Driven Condition Monitoring Approaches to Improving Power Output of Wind Turbines. *IEEE Trans. Ind. Electron.* **2019**, *66*, 6012–6020.
27. Guo, Q.; Huang, C.; Xue, Z. Multi-Objective Optimization of Wind Farm Dispatch Problem by Double-Layer Particle Swarm Optimization Algorithm. In Proceedings of the 2019 IEEE 8th Data Driven Control and Learning Systems Conference (DDCLS), Dali, China, 24–27 May 2019; pp. 728–733.
28. Xiao, T.; Chen, Y.; Huang, S. Feasibility Study of Neural ODE and DAE Modules for Power System Dynamic Component Modeling. *IEEE Trans. Power Syst.* **2023**, *38*, 2666–2678.
29. Rao, Y.; Lyu, J.; Cai, X. Wideband impedance online identification of wind farms based on combined data-driven and knowledge-driven. In Proceedings of the 2022 IEEE International Power Electronics and Application Conference and Exposition (PEAC), Guangzhou, China, 4–7 November 2022; pp. 533–538.
30. Wang, Z.; Lv, J.; Cai, X. Data-driven impedance identification and stability analysis of doubly-fed induction generator based wind turbines. *Electr. Power Constr.* **2023**, *44*, 31–40.
31. Sun, J. Impedance-based stability criterion for grid-connected inverters. *IEEE Trans. Power Electron.* **2011**, *26*, 3075–3078.
32. Hochreiter, S. The vanishing gradient problem during learning recurrent neural nets and problem solutions. *Int. J. Uncertain. Fuzziness Knowl.-Based Syst.* **1998**, *6*, 107–116. [CrossRef]
33. Li, S.; Kong, R.; Blaabjerg, F.; Anvari-Moghaddam, A. Sequence Impedance Prediction for Grid-Connected Converters Based on Bi-LSTM. *IEEE Trans. Power Electron.* **2025**, early access. [CrossRef]
34. He, K.; Zhang, X.; Ren, S.; Sun, J. Deep Residual Learning for Image Recognition. In Proceedings of the IEEE Conference on Computer Vision and Pattern Recognition (CVPR), Las Vegas, NV, USA, 27–30 June 2016; pp. 770–778.

35. Kundur, P. *Power System Stability and Control*; McGraw-Hill: New York, NY, USA, 1994.
36. Blaabjerg, F.; Teodorescu, R.; Liserre, M.; Timbus, A.V. Overview of Control and Grid Synchronization for Distributed Power Generation Systems. *IEEE Trans. Ind. Electron.* **2006**, *53*, 1398–1409. [CrossRef]
37. Bergstra, J.; Bengio, Y. Random Search for Hyper-Parameter Optimization. *J. Mach. Learn. Res.* **2012**, *13*, 281–305.
38. Raissi, M.; Perdikaris, P.; Karniadakis, G.E. Physics-Informed Neural Networks: A Deep Learning Framework for Solving Forward and Inverse Problems Involving Nonlinear Partial Differential Equations. *J. Comput. Phys.* **2019**, *378*, 686–707. [CrossRef]
39. Kingma, D.P.; Ba, J. Adam: A Method for Stochastic Optimization. In Proceedings of the 3rd International Conference on Learning Representations (ICLR), San Diego, CA, USA, 7–9 May 2015.

Disclaimer/Publisher's Note: The statements, opinions and data contained in all publications are solely those of the individual author(s) and contributor(s) and not of MDPI and/or the editor(s). MDPI and/or the editor(s) disclaim responsibility for any injury to people or property resulting from any ideas, methods, instructions or products referred to in the content.